Cerebral Cortex 2007;17:i16-i26
doi:10.1093/cercor/bhm103

Cannabinoid-Mediated Disinhibition and Working Memory: Dynamical Interplay of Multiple Feedback Mechanisms in a Continuous Attractor Model of Prefrontal Cortex

Eugene Carter[1] and Xiao-Jing Wang[1,2]

[1]Department of Biology, Brandeis University, Waltham, MA 02454-9110, USA and [2]Department of Neurobiology, Yale University School of Medicine, New Haven, CT 06510, USA

Recurrent excitation is believed to underlie persistent neural activity observed in the prefrontal cortex and elsewhere during working memory. However, other positive and negative feedback mechanisms, operating on disparate timescales, may also play significant roles in determining the behavior of a working memory circuit. In this study, we examined dynamical interactions of multiple feedback mechanisms in a biophysically based neural model of spatial working memory. In such continuous attractor networks, a self-sustained activity pattern tends to drift randomly, resulting in a decreased accuracy of memory over time. Moreover, attractor states become unstable when spike-frequency adaptation reduces the excitability of persistently firing pyramidal neurons. Here, we show that a slow activity-dependent local disinhibition, namely cannabinoid-dependent depolarization-induced suppression of inhibition (DSI), can counteract these destabilizing effects, rendering working memory function more robust. In addition, the slow DSI effect gives rise to trial-to-trial correlations of memory-guided behavioral responses. On the other hand, computer simulations revealed that a global cannabinoid agonist (mimicking the effect of drug intake) yields the opposite effect. Thus, this work suggests a circuit scenario according to which endogenous DSI is beneficial for, whereas an exogenous drug such as marijuana is detrimental to, working memory and possibly other prefrontal functions.

Keywords: continuous attractor network, endocannabinoid, oculomotor delayed-response task, prefrontal cortex, working memory

Introduction

Working memory, the ability to actively hold information "on-line" in the absence of direct external inputs, enables the brain to delay responses to sensory stimuli so that information can be integrated and complex behaviors can be organized flexibly across time. The prefrontal and parietal cortices play a critical role in working memory, as demonstrated by electrophysiological experiments with nonhuman primates (Fuster 1973; Niki and Watanabe 1976; Gnadt and Andersen 1988; Funahashi et al. 1989; Chafee and Goldman-Rakic 1998; Rainer et al. 1998; Romo et al. 1999; Sawaguchi and Yamane 1999; Kikuchi-Yorioka and Sawaguchi 2000; Sawaguchi and Iba 2001; Takeda and Funahashi 2002), brain imaging (McCarthy et al. 1994; Courtney et al. 1998; Zarahn et al. 1999), and transcranial magnetic stimulation studies (Müri et al. 1996; Oliveri et al. 2001; Koch et al. 2005). An elegant and widely used spatial working memory paradigm is the oculomotor delayed-response (ODR) task, in which the subject is required to remember the spatial location of a visual cue across a delay period (typically of a few seconds) in order to perform a memory-guided saccadic response. Funahashi et al. (1989) found that single neurons in the dorsolateral prefrontal cortex (PFC) and frontal eye field exhibited elevated persistent activity during the delay period, even though the stimulus was no longer present. This mnemonic activity was spatially selective according to a Gaussian-shaped tuning curve and, therefore, could be used to guide a delayed saccadic response.

To investigate the neural circuit mechanism of stimulus-selective persistent activity underlying working memory, we have developed a biophysically constrained network model of spiking neurons for the ODR experiment (Camperi and Wang 1998; Compte et al. 2000; Renart et al. 2003). This model is endowed with a Mexican-hat architecture (Amari 1977; Ben-Yishai et al. 1995), with local excitation between pyramidal cells with similar spatial preference and broad synaptic inhibition from γ-aminobutyric acidergic (GABAergic) cells. When the strength of recurrent excitatory synapses is sufficiently strong, the network exhibits bell-shaped persistent activity patterns (or bump attractors) that can store the memory of a spatial location as an analog quantity. These mnemonic states coexist with a spontaneously active baseline state, so that the network can be switched on and off by brief external inputs, as required for a working memory system. We found that in this model, working memory function depends on the slow *N*-methyl-D-aspartate receptors at the recurrent synapses and the balance between synaptic excitation and inhibition (Wang 2001, 2006; Constantinidis and Wang 2004). Furthermore, heterogeneity in cellular properties was shown to destroy the continuous family of bump attractors, but the latter could be restored with the introduction of a compensatory, homeostatic synaptic scaling mechanism (Renart et al. 2003).

The continuous nature of an attractor network generally gives rise to random drifts of a persistent activity pattern (Camperi and Wang 1998; Compte et al. 2000). This implies that the remembered spatial cue, hence the memory-guided saccade, becomes less precise with a longer delay. Moreover, it has been shown previously that spike-rate adaptation (SRA), a common property of cortical pyramidal neurons, weakens the excitability of those cells that fire in a sustained manner, leading a bump attractor to either move across the network as a propagating wave or disappear quickly (Hansel and Sompolinsky 1998; Laing and Longtin 2001; Pinto and Ermentrout 2001a, 2001b). Consequently, memory storage can no longer be maintained. SRA-induced negative feedback in single cells cannot be simply compensated by an increased strength of fast synaptic excitation because the interplay between the 2 processes often gives rise to oscillatory instabilities (Wang 1999; van Vreeswijk and Hansel 2001), as can be intuitively expected for a strongly nonlinear dynamical system with a fast positive feedback and a slower negative feedback. In the present study, we tested the hypothesis that persistent activity can be stably maintained in spite of certain amount of SRA, if the latter is counteracted by an

activity-dependent excitation or disinhibition that operates on a slower timescale. Specifically, we examined such a mechanism in our spatial working memory model, namely the cannabinoid-mediated depolarization-induced suppression of inhibition (DSI).

DSI was first discovered in Purkinje cells in the cerebellum by Llano et al. (1991) and pyramidal cells in the hippocampus by Pitler and Alger (1992). Pitler and Alger evoked action potentials at 20 Hz for 2 s in CA1 pyramidal cells and found that the size and frequency of subsequent spontaneous inhibitory events were reduced for 10–20 s. This phenomenon has been observed in pyramidal cells of the PFC (Trettel and Levine 2003; Fortin et al. 2004; Bodor et al. 2005) and hippocampus (Pitler and Alger 1992) as well as the Purkinje cells of the cerebellum (Llano et al. 1991; Brenowitz and Regehr 2003). DSI has been found to be mediated, at least in part, by endogenous cannabinoids (Ohno-Shosaku et al. 2001; Wilson and Nicoll 2001; Wilson et al. 2001). In the brain, endocannabinoid signaling is primarily mediated by G-protein–coupled CB1 receptor. CB1 receptors appear to be predominantly located on the axon terminals of a subtype of GABAergic cells that contain the neuropeptide cholecystokinin (CCK) (Katona et al. 1999; Marsicano and Lutz 1999; Bodor et al. 2005; Eggan and Lewis 2007) and target the perisomatic region of pyramidal cells (Katona et al. 1999; Klausberger et al. 2005). Physiological experiments (Hajos et al. 2000; Hoffman and Lupica 2000; Kreitzer and Regehr 2001; Ohno-Shosaku et al. 2001; Wilson and Nicoll 2001; Wilson et al. 2001) show that DSI is triggered by calcium influx in a pyramidal neuron, leading to the release of endogenous cannabinoids which, through a retrograde signal, activate CB1 receptors at the presynaptic terminal from CCK neurons. The activation of CB1 causes a reduction in the release probability of transmitter GABA. As a result, the pyramidal cell is disinhibited. Wilson and Nicoll tested the effective radius of DSI and found that the spatial spread is not more than 20 μ from the depolarized neuron (Wilson et al. 2001).

There is a large body of literature documenting that cannabinoid has a significant effect on a range of cognitive behaviors. The primary psychoactive constituent of the hemp plant *Cannabis sativa*, 9-D-tetrahydrocannabinol (THC), has been found to impair working and episodic memories (Ameri 1999; Hampson and Deadwyler 2000; Ploner et al. 2002; Ilan et al. 2004). Of particular interest here is the study by Ploner et al. (2002), in which human subjects performed an ODR task. It was found that when subjects take an exogenous cannabinoid (THC), the accuracy of memory-guided saccade decreases compared with the control condition. CB1 receptor is highly expressed in the PFC (Glass et al. 1997; Ong and Mackie 1999; Dean et al. 2001; Eggan and Lewis 2007), especially in layer 2/3 (Eggan and Lewis 2007), which is endowed with an abundance of recurrent connections and has been hypothesized to be a neural substrate for working memory (Goldman-Rakic 1995). Therefore, endocannabinoid signaling is well positioned to modulate prefrontal processes. In this study, we incorporated the DSI effect into our spatial working memory model to investigate precisely how cannabinoid signaling affects cognition.

Methods

A Simple Model of the DSI Phenomenon

The current understanding of the mechanism of DSI has been reviewed in Alger and Pitler (1995), Wilson and Nicoll (2002), and Freund et al. (2003). Briefly, depolarization secondary to action potentials or voltage clamping causes influx of calcium (Llano et al. 1991; Pitler and Alger 1992; Lenz and Alger 1999). The increase in intracellular calcium in turn causes the production of endocannabinoid (Di Marzo et al. 1994; Stella et al. 1997; Piomelli 2003). Once produced, endocannabinoids mediate a retrograde signaling at the presynaptic terminals from CCK neurons onto the depolarized pyramidal cell, but the detailed mechanism of retrograde transport is still unclear. At the presynaptic side, endocannabinoids bind to the CB1 receptor, which causes a reduction in presynaptic release probability (Hajos et al. 2000; Hoffman and Lupica 2000; Kreitzer and Regehr 2001; Ohno-Shosaku et al. 2001; Wilson and Nicoll 2001; Wilson et al. 2001). The mechanism for endocannabinoid clearance is yet to be worked out, but cannabinoids appear to undergo either facilitated transport or passive diffusion to reenter the cells where they are then hydrolyzed (Freund et al. 2003; Piomelli 2003).

Our phenomenological model of DSI was designed to capture quantitatively 2 most salient observations: the dependence on intracellular calcium and the slow decay time course (which appears to correspond to the deactivation process [Heinbockel et al. 2005]). We assumed that the inhibitory synaptic conductance g_{GABA} on a pyramidal cell is multiplied by a factor D, which is proportional to the fraction of inhibitory synapses that are sensitive to cannabinoid and their presynaptic release probability (D is between 0 and 1; $D = 1$ when there is no DSI effect). In most studies, DSI is reported as the percent reduction in inhibitory event size (or frequency). Thus, the relationship between DSI and D is DSI = 100 × (1 − D).

The dynamics of D is described by the following equation:

$$\frac{dD}{dt} = \phi_D \times \left(\frac{1-D}{\tau_D} - \beta_D \times [Ca^{2+}]^n \times (D - D_{min}) \right), \quad (1)$$

where $[Ca^{2+}]$ represents the intracellular calcium concentration in the pyramidal cell. When $[Ca^{2+}]$ accumulates, D decreases with a rate controlled by β_D, causing disinhibition. The parameter n is the cooperativity factor which was used to fit the model with physiological data (see below), and was set to one for all the model simulations. D is bounded below at D_{min}, which determines the maximum disinhibition and biophysically corresponds to the maximum number of synapses that are cannabinoid sensitive multiplied by the maximal reduction in release probability at each synapse due to DSI. When the pyramidal cell ceases to be active, D recovers back to maximal value one with a time constant τ_D. The factor ϕ_D represents temperature sensitivity.

Based on the observation that calcium entry is through high-threshold calcium channels (Lenz and Alger 1999; but see Isokawa and Alger 2006), we assumed that $[Ca^{2+}]$ influx is triggered by spikes and obeys a first-order kinetics as follows (Liu and Wang 2001):

$$\frac{d[Ca^{2+}]}{dt} = -\frac{[Ca^{2+}]}{\tau_{Ca}} + \alpha_{Ca} \times \sum \delta(t - t_i).$$

When an action potential fires (at time t_i), $[Ca^{2+}]$ is incremented by α_{Ca}. The calcium concentration decays back to zero exponentially with a time constant τ_{Ca}. The values for α_{Ca} and τ_{Ca} were chosen to model calcium behavior in the soma as the axon terminals expressing CB1 appear to be concentrated in the perisomatic region (see Introduction). The values for α_{Ca} (0.2 μM) and τ_{Ca} (240 ms) are the same as in Liu and Wang (2001) and Wang et al. (2003) and calibrated by experimental measurements (Schiller et al. 1995; Helmchen et al. 1996).

We constrained the parameter values of our model by data published in Wang and Zucker (2001). Their experiments were conducted at 24 °C on CA1 pyramidal cells from rat (11–22 postnatal day) hippocampal slices. Calcium influx was generated by voltage clamping the cells to 0 mV and was monitored via the calcium-sensitive dye benzothiazole coumarin (BTC). DSI was calculated from the amplitude of evoked inhibitory postsynaptic currents (IPSCs) before and after depolarization. The magnitude of DSI generated was varied by using different lengths of depolarizations. Once DSI was initiated, they directly measured τ_D, which yielded 16.7 s. Moreover, they calculated the relationship between peak DSI and peak calcium concentration, which we used to

estimate the parameter β_D. Solving the steady state of equation (1), one obtains

$$DSI_{ss} = \frac{DSI_{MAX} \times [Ca^{2+}]^n}{K_{50} + [Ca^{2+}]^n},$$

where

$$K_{50} = \frac{1}{\beta_D \times \tau_D}$$

n and K_{50} were measured to be 1.36 and 3.9 μM (Wang and Zucker 2001). Using $\tau_D = 16.7$ s, we deduce $\beta_D = 1.66\ 10^{-5}$ (μM ms)$^{-1}$. This way, the model parameters have been well constrained by experimental measurements. We did not attempt to capture the slow time course of $[Ca^{2+}]$ measured by Wang and Zucker (2000), which could be partly caused by calcium-induced calcium release from internal stores (Isokawa and Alger 2006) and possibly partly due to the buffering effect of the calcium-sensitive dye BTC.

Our $[Ca^{2+}]$ model is spike based and does not automatically describe calcium influx by constant membrane potential depolarization. To mimic the experiment with the voltage clamped at 0 mV, we implemented calcium as having a constant rate (χ) of influx during depolarization, consistent with the experimental data of Thayer and Miller (1990) and Brenowitz and Regehr (2003). With χ taken to be 0.00125 μM/s, this model captures well the experimentally observed relationship between DSI and calcium (Fig. 1*B*) and the raw time course data from one cell (Fig. 1*C*). Note that to fit data from a single cell, the model parameters used differed from the "average" values given above.

The experimental data we used to fit the model were collected at 24 °C. On the other hand, the working memory model simulations are meant to represent physiological process occurring at monkey's body temperature. It has been reported that DSI signaling is temperature dependent (Kreitzer et al. 2002; Heinbockel et al. 2005). Kreitzer et al. (2002) examined the temperature dependence of DSI at climbing and parallel fibers in the cerebellum. Using the more conservative of the values measured at the 2 types of fibers, we calculated Q_{10} to be 3.0. We used this value as ϕ_D (representing 34 °C) so that τ_D is effectively 5.57 s. This value is consistent with Heinbockel et al. (2005), who performed measurements at 30 °C on hippocampal slices.

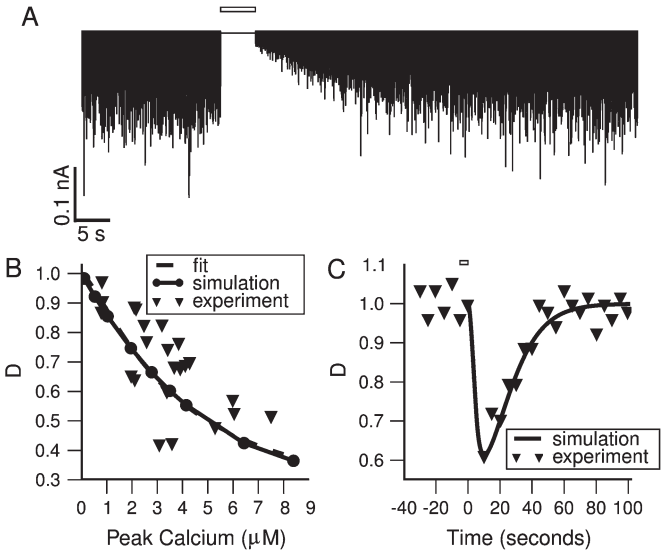

Figure 1. A phenomenological model of depolarization-induced suppression of inhibition. (*A*) Model simulated IPSCs from a 100-Hz Poisson spike train before and after DSI induction by a 5 s depolarization (open bar). Note the reduction in IPSC amplitude and slow recovery. (*B*) Dependence of minimum *D* (maximum DSI) on peak calcium concentration. Calcium influx was triggered by depolarization to 0 mV. Experimentally, DSI was measured by comparing the amplitudes of evoked IPSCs before and after depolarization. Triangles: experimental data from (Wang and Zucker 2001) Figure 4 (converted to *D*). Dashed line: data fitting to a Hill equation; filled circles: model simulations; solid line: the Hill equation from our model. (*C*) Sample time course of DSI after a 5-s depolarization (open bar). Triangles: experimental data from Figure 3 of Wang and Zucker (2001), after conversion to *D*; solid line: model simulation results.

Spike-Rate Adaptation

We investigated the interaction between DSI and SRA (McCormick et al. 1985; Mason and Larkman 1990; Foehring et al. 1991) in our spatial working memory model. In our studies, adaptation was modeled as a potassium current due to calcium concentration (Liu and Wang 2001): $I_{AHP} = g_{AHP} \times [Ca^{2+}] \times (V - E_K)$. The g_{AHP} controls the amount of adaptation and is varied as a parameter. E_K is the potassium equilibrium potential and is set to –80 mV. We quantified the amount of SRA by F_{adapt}, which was calculated as 100 × (initial rate – steady state rate)/initial rate. In order to convert g_{AHP} into F_{adapt}, we ran single-cell simulations with a fixed g_{AHP} and a range of injected current intensity. We calculated F_{adapt} from the simulation where the final rate was ~35 Hz.

Recurrent Network Model of Spiking Neurons

The network model in this study has been previously described in detail (Compte et al. 2000), and unless stated otherwise, we used the same parameters as in Compte et al. (2000). The model consists of 2 populations of leaky-integrate-and-fire model neurons (Tuckwell 1988). The excitatory population consists of 2048 neurons, whereas the inhibitory population has 512 neurons. A schematic of the network structure is shown in Figure 2*A*. Pyramidal cells are labeled by their preferred saccade direction from 0 to 360 degrees. The excitatory-to-excitatory connections have a Gaussian weight profile, so that neurons with similar stimulus preference are strongly connected with each other. All the other recurrent connections are unstructured, for the sake of simplicity. All the model neurons receive strong, random background fluctuations as well as full recurrent connections. The network reproduces the salient features of the electrophysiological observations from primates performing the ODR (Funahashi et al. 1989) spatial working memory task (Compte et al. 2000). To this model, we added the features of DSI and SRA as described above. In the original model, for each pyramidal cell *i*, the inhibitory current is calculated as

$$I_{inh,i} = g_{GABA,i} \times \sum^{Inhpool} s_{GABA} \times (V_i - E_{Cl}).$$

In this study, $g_{GABA,i}$ is multiplied by a factor D_i for each pyramidal cell *i*. D_i is determined by the postsynaptic activity and applies only to the inhibitory input in the same pyramidal neuron.

All the model parameters are the same as the "modulated parameter set" used in Compte et al. (2000). In simulations of the effect of a global cannabinoid agonist (Fig. 6), the inhibitory-to-excitatory synaptic conductance g_{GABA} was increased by 0.5%.

Model Implementation

The model was integrated with the Runge–Kutta second order algorithm with the firing time interpolation scheme (Hansel et al. 1998) using a time step of 0.02 ms. The code was written in C and run on AMD opteron processors.

Analysis of Simulation Data

To facilitate visualization, in a single-trial simulation, we created spatiotemporal maps of firing rate and *D*. To compute the firing rate map, we sorted the spike trains by cell label and time. We then convolved that result with a boxcar filter (generally of 10 cells by 50 ms). The values produced were then mapped onto a color scale and plotted as a spatiotemporal pattern. In order to determine the peak location of a bell-shaped persistent firing pattern, we utilized the population vector method (Georgopoulos et al. 1982). The value for *D* was recorded for every cell averaged over 50-ms time bins. These values were converted to a map in the same manner as the firing rate map though without the convolution step. The population vector method was again used to compute the peak location of the DSI disinhibition.

To assess the accuracy of memory-guided saccade in the model, we used the method described in Renart et al. (2003) for calculating the 2-dimensional saccade endpoint.

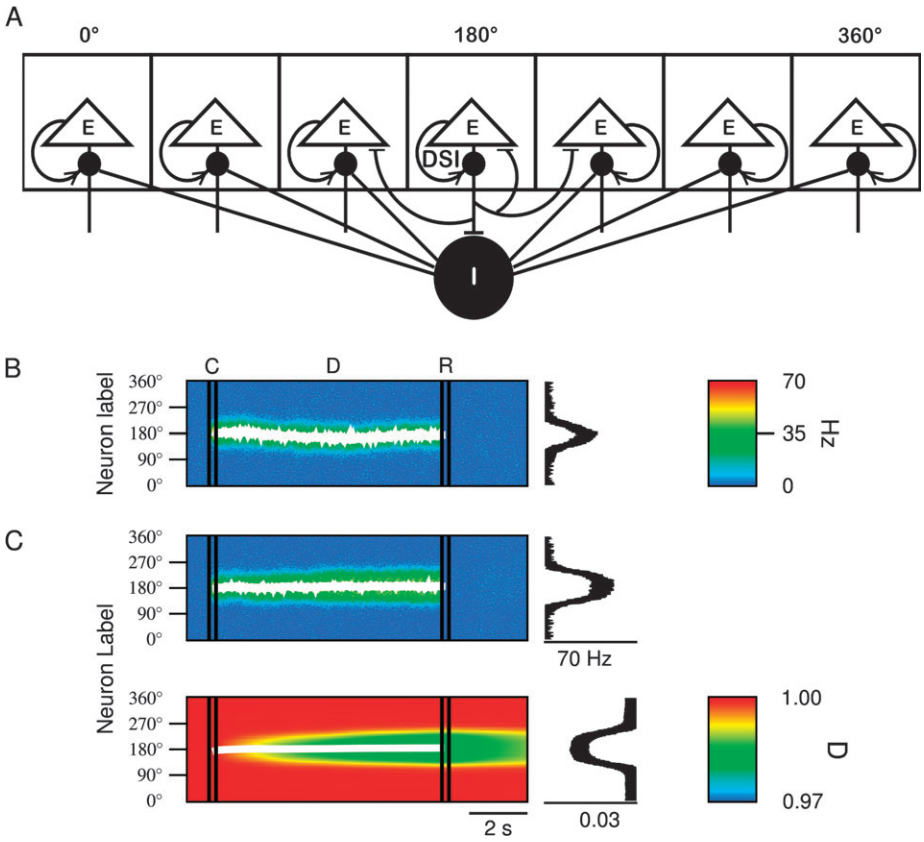

Figure 2. Network model of spatial working memory endowed with DSI. (*A*) Schematic network architecture. Excitatory cells are labeled and arranged by their preferred cues (0–360 degrees). Excitatory-to-excitatory connections are structured such that pyramidal cells with similar preference are more strongly connected to each other. The connections from the inhibitory population to itself as well as to the excitatory population are unstructured. DSI is implemented as a cell-specific reduction in inhibitory input conductance. (*B*) Model simulation of the ODR task without DSI. The spatiotemporal network activity pattern is shown with a color-coded firing rate map (see color bar); the abscissa is time and the ordinate is neuron label. The white line represents the stored cue location as the peak location of a bell-shaped persistent activity pattern, measured by the population vector. The network activity profile averaged over the last half second of the delay period is shown on the right. (*C*) Spatiotemporal network activity with DSI. Top: firing rate activity; Bottom: DSI activity ($D_{min} = 0.97$). The white line represents the dip location of the *D* population pattern. The *D* profile (on right) was calculated by averaging *D* over the last half-second of the delay period. Note the slow buildup and decay of the DSI effect at the same location as the neural spiking activity.

Results

DSI Creates a Footprint of Disinhibition

Network simulations were carried out according to the ODR protocol of Funahashi et al. (1989), with each trial consisting of a cue period (C) when the stimulus is presented and encoded, a delay period (D) when the cue location must be remembered, and a response period (R) when the memory is retrieved to produce a behavioral response. In the simulations shown below, the network activity is displayed in the form of a color-coded spatiotemporal firing rate map. Figure 2*B* shows the model behavior without DSI. The network is initiated in a spontaneously active baseline state. A brief (250 ms) external input localized at 180 degrees triggers elevated activity in a group of neurons at the center of the network. This activity pattern is self-sustained by virtue of recurrent excitation during the delay period. At the end of the delay period, a 250-ms current injection in the inhibitory population turns off the persistent activity and switches the network back to the baseline state. During the delay period, the remembered cue is given by the peak location, measured by the population vector (Georgopoulos et al. 1982), of the network activity profile as a function of time (white line in Fig. 2*B*). On the right of the spatiotemporal pattern is shown the network activity profile, averaged over the last half second of the delay period, which exhibits a bell-shaped persistent activity pattern.

Figure 2*C* shows a network simulation when DSI is turned on, as shown by a spatiotemporal map of *D* at the bottom of the panel *C* (recall that physiologically measured DSI is related to *D* by DSI = (1 – *D*) × 100%). When the trial starts, pyramidal cell firing rate is low and *D* is essentially 1. During the cue period, *D* does not change significantly due to the latency of DSI. The elevated firing activity in the activated cells slowly causes a reduction in *D* during the delay period, creating a footprint of disinhibition. *D* decreases through the delay period of 8 s. After the termination of firing rate activity in the response period, *D* lingers on as its decay time constant is 5.57 s. This leaves a "memory trace" in the network for several seconds after firing rate activity has ceased. The population profile of *D* takes the shape of a shallow well (Fig. 2*C*, bottom panel on the right). The depth of the well slowly increases during the delay period. The white line plotted during the delay period represents the location of the minimum *D* (maximum DSI) as calculated from the population vector (see Methods). Comparing the firing rate and *D* maps in Figure 2*C*, it can be seen that the location of the firing rate bump coincides with the location of maximal DSI.

The variation of *D* is small (a few percent), but this modest DSI affects the network behavior quite significantly, as can be

seen by comparing Figure 2*B,C*. Without DSI, the network activity profile's shape stays approximately the same throughout the delay period but the remembered location drifts randomly (the population vector is not a perfectly horizontal line in panel *B*). Adding DSI causes the network activity profile to change, increasing in amplitude and widening, over time. The peak of the activity profile in Figure 2*B* is 32 Hz, with a width of 28 degrees as measured by fitting with a Gaussian. With DSI (Fig. 2*C*), the peak is 49 Hz, with a width of 39 degrees. The shape of the network activity profile with DSI becomes more square-like as the delay period progresses (the network eventually reaches a steady state that generally occurs after 20 s). The increase in amplitude and width takes place in parallel with the gradual development of DSI: firing activity causes a slow disinhibition; disinhibition increases the excitability, which in turn enhances neural activity. Comparing the firing rate activity map with the *D* map, it can be seen that the population vectors for the firing and *D* patterns occur at the same location. Even though the shape of the bump attractor changes over time, the location of the peak does not, suggesting that encoded memories are more stable and accurate in our model with DSI.

Random Drifts and Memory Accuracy

The quality of memory maintenance over time is measured by plotting the population vector (remembered location) over time for a number of trials with the same stimulus. This is shown in Figure 3*A* without DSI (left panel), as reported previously (Compte et al. 2000; Renart et al. 2003). It can be seen that the population vector deviates from the stimulus cue as in a random walk so that the trial average is zero and the variance grows approximately linearly with time during a delay period of 6 s (Fig. 3*B*, gray trace). Random drifts occur because the cue-triggered bump attractor is one of many in a continuous family. During a delay period there is no external bias, synaptic noise and irregular neural activity induce stochastic shifts among this continuum of persistent activity patterns.

We found that the addition of DSI greatly reduced random drifts of persistent activity during the delay. This is shown in Figure 3, where it can be seen that with DSI the population vector time courses remain confined in a narrow band (panel *A*, right) and the variance of the remembered location remains limited over time (panel *B*, black trace). Note that the variance is similar with or without DSI for the first 2 s because of the slow onset of the disinhibition well (Fig. 2*C*). DSI suppresses random drifts by producing a "privileged" network location to "trap" a persistent firing pattern. The crucial requirement for this mechanism to work is that DSI is activity dependent and spatially localized. In our spatial working memory model, a bump of neural activity causes disinhibition for those neurons selective for the presented cue. The increased activity of pyramidal cells also generates, via interneurons, an increased (lateral) inhibition to the network as a whole, which forms a barrier that resists the movement of the bump from network locus of low inhibition to elsewhere. Thus, by reducing random drifts of mnemonic activity, DSI increases the accuracy of memory-guided saccadic responses.

Working Memory Function in the Presence of Spike-Rate Adaptation

Previous work has shown that a continuous attractor network can be destabilized if persistently active cells become less

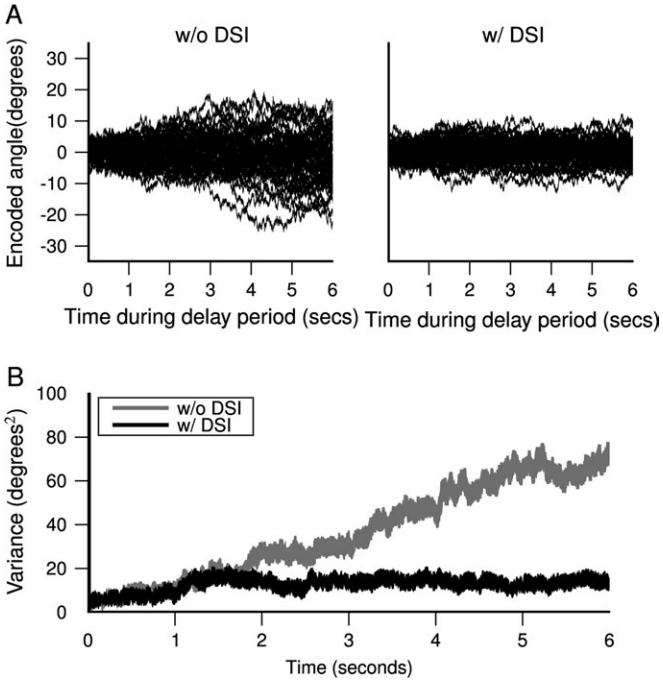

Figure 3. DSI enhances the accuracy of memory-guided responses by reducing random drifts of persistent activity. (*A*) Time course of remembered cue location (determined by the population vector) throughout a delay period of 6 s, for 50 trials. Left: without DSI. Right: with DSI (D_{min} = 0.97). (*B*) Variability of remembered cue location as a function of time, calculated as the variance of the population vector across 50 trials in (*A*). Without DSI the variance of the population vector grows in time (gray line). DSI creates a privileged locus to stabilize a mnemonic activity pattern, so that after an initial increase in the first 2 s, the variance plateaus and remains constant (black line).

excitable over time, for instance, due to SRA (Hansel and Sompolinsky 1998; Laing and Longtin 2001). SRA refers to a gradual decrease of a single neuron's firing rate in response to a constant input current. It is a feature of pyramidal cells commonly observed in cortical slices (Connors et al. 1982; McCormick et al. 1985; Mason and Larkman 1990; Foehring et al. 1991; Lorenzon and Foehring 1992). We implemented SRA in single pyramidal cells of our model, as in Liu and Wang (2001), where spiking activity induces influx of calcium, which activates a slow potassium conductance (see Methods). Consistent with previous studies (Laing and Longtin 2001), reduction in excitability due to SRA abolishes persistent activity (Fig. 4*A*). This happens with very small SRA (quantified by F_{adapt} = 100 × (initial rate – steady state rate)/initial rate ~4%). We reasoned that DSI represents a well-suited mechanism to counteract SRA as SRA is a cellular process of activity-dependent reduction in excitability, whereas DSI is an activity-dependent disinhibition (with a longer time constant). This is indeed the case: we found that persistent activity was restored with the addition of the DSI effect, as can be seen in Figure 4*B* with F_{adapt} ~10% and D_{min} = 0.96. Smaller values of D_{min} can compensate for a larger amount of adaptation, but too much DSI could make the baseline state unstable, leading to spontaneous emergence of persistent activity without any stimulus. Interestingly, in the presence of both DSI and adaptation in the network, the network activity profile is more Gaussian-like in shape than with DSI alone (Fig. 4*B*, with a height of 35 Hz and a width of 30 degrees).

Moreover, it has been reported (Hansel and Sompolinsky 1998; Laing and Longtin 2001) that in a bump attractor network

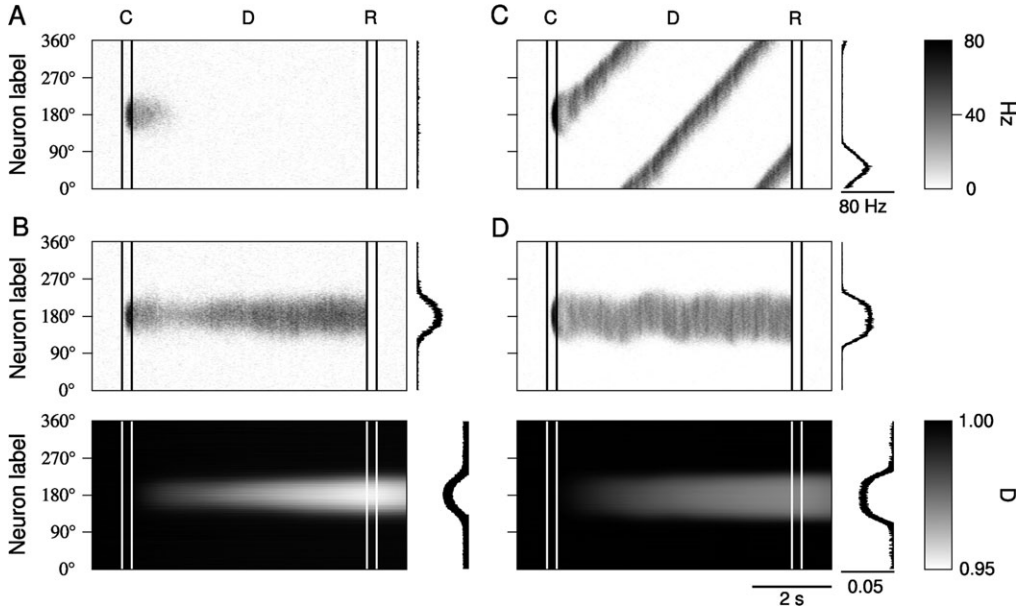

Figure 4. SRA destabilizes working memory function, which is restored by DSI. (*A*) Spatiotemporal activity pattern without DSI. The addition of a small amount of SRA (g_{AHP} = 0.0006) causes a cue-triggered activity pattern to decay within 1 s so the memory is lost. (*B*) Disinhibition by DSI (D_{min} = 0.96) counteracts SRA and rescues the self-sustained persistent activity. Spatiotemporal activity pattern (top) and spatiotemporal DSI (bottom) are shown in gray scales. (*C*) Spatiotemporal network activity without DSI and with a high signal to noise ratio. A significant amount of SRA (g_{AHP} = 0.005 that yields F_{adapt} = 50%) causes the delay activity to move as a propagating wave, so the memory can no longer be retrieved. (*D*) Spatiotemporal activity (top) and spatiotemporal DSI (bottom) with the same parameters as (*C*), but with the addition of DSI (D_{min} = 0.95). Activity-induced well of disinhibition compensates for SRA and prevents the activity pattern from traveling away from the initial cue location.

with low noise, adaptation induces a persistent firing pattern to propagate across the network as a wave. This was confirmed in our study when we doubled the strength of recurrent synapses (see Fig. 4*C*). What happens is that the hyperpolarizing effect of SRA reduces activity of neurons in a bump state, and at the same time, recurrent activity spreads the activity to neighboring neurons less encumbered by SRA. Noise breaks the symmetry so the network activity shifts to either the left or right. Because the neurons from which the activity pattern has just shifted way are less excitable, the bump will continue to travel in one direction. Again, as expected, the persistent activity was rescued by the addition of the DSI effect. This is shown in Figure 4*D* with D_{min} = 0.95, where one sees that the bump attractor is stabilized at the location of the disinhibition footprint (a smaller value for D_{min} was utilized to compensate for the destabilizing effect of SRA).

Intertrial Interval Effects

Although the slow time constant of DSI contributes to the stabilization of memories, it also creates a footprint of disinhibition that lingers after the network firing activity has been terminated at the end of a trial. If intertrial intervals are not too long, the lingering spatially localized disinhibition from the previous trial would influence persistent activity in the current trial, leading to correlated behavioral responses from one trial to the next. To examine this possibility we simulated two consecutive trials, using a fixed cue (θ_1) at 180 degrees in the first trial and a delay period of 3 s. The persistent activity was switched off at the end of the first trial, as described earlier. After an intertrial interval of variable length, in the next trial a second cue was presented to the network at θ_2. To assess the cross-trial effect, we looked at the remembered cue location θ_{pop} at the end of the delay period in the second trial. The spatiotemporal firing rate map of a sample simulation is shown in Figure 5 (top panel). Clearly, in the second trial, the encoded location by persistent activity shifts back toward θ_1, the cue location in the previous trial. This is because when in the second trial the persistent activity is initiated, there is already a network region of weak disinhibition inherited from the previous trial. If neurons in this more excitable location are near the bump attractor, the latter will be biased toward the well of disinhibition, leading to a systematic shift (unlike random drift by noise) of the bump attractor. We examined the dependence of this effect on the distance $\theta_1 - \theta_2$. Figure 5 (middle panel) shows that the systematical shift (measured by $\theta_2 - \theta_{pop}$) is at maximum when the distance between the first and second cues are neither too small nor too large (when the interaction is weak between second firing rate bump and the previously generated well of disinhibition). This is also shown in Figure 5 (bottom panel), where we plotted $\theta_2 - \theta_{pop}$ as a function of the intertrial interval duration. The systematic shift is larger with $\theta_2 - \theta_1 = 90$ degrees than 45 degrees or 135 degrees. Furthermore, as expected, the trial-to-trial effect is smaller with a longer intertrial interval when the DSI has more time to decay away between the 2 trials.

Global Agonist

Our finding that DSI enhances spatial working memory is in contrast to Ploner et al. (2002), who reported that human subjects show less accurate memory-guided saccades when exposed to THC (the main psychoactive constituent of marijuana) compared with the control condition. We reasoned that the discrepancy could be explained by the difference between endogenous cannabinoid signaling, which is local and activity dependent and an exogenous cannabinoid mediating a global and activity-independent action. Therefore, we set out to

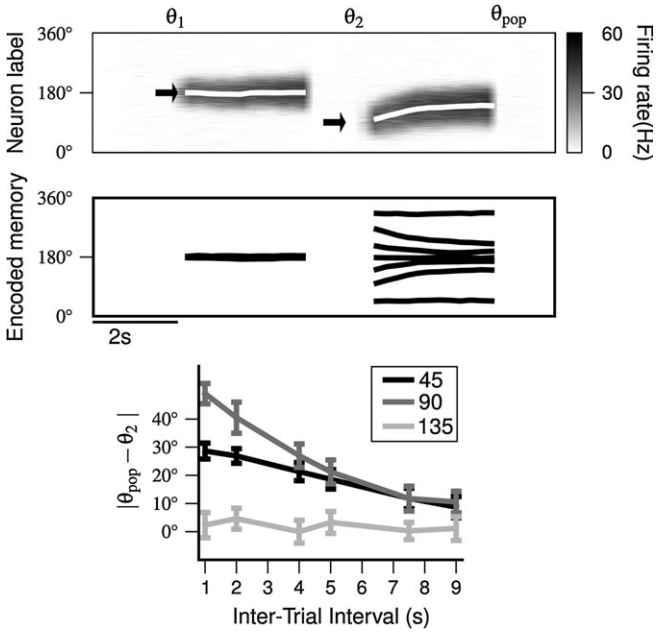

Figure 5. Trial-to-trial effects by stimulus-specific and long-lasting DSI. Top panel: spatiotemporal activity pattern illustrating the simulation protocol. Two cues were presented; the first (θ_1) cue was presented for 0.25 s, followed by a 3 s delay period, and then a 0.25 s termination period. After a 1-s intertrial interval, another cue (θ_2) was presented. Arrows indicate cue locations. The white lines are the remembered locations measured by population vector. The θ_{pop} denotes the remembered location at the end of the second delay. Middle panel: population vector over time for various values of θ_2. Bottom panel: systematic drift of population vector versus intertrial interval, for 3 different values of θ_2 so that $|\theta_1 - \theta_2| = 45$, 90, and 135 degrees, respectively. Note larger drifts when the 2 cues in the consecutive trials are separated by 90 degrees than when they are 45 degrees apart because in the latter case there is less space for the activity pattern in the second trial to travel toward the cue location in the first trial. When 135 degrees or more separates the cues, there is no interaction between consecutive cues. In all simulations D_{min} is 0.97.

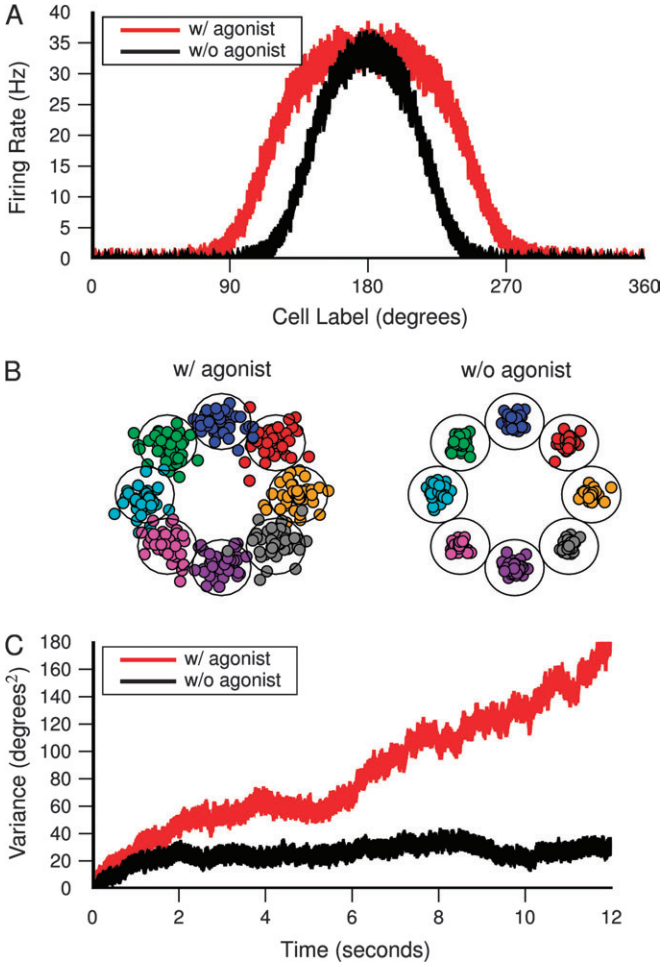

Figure 6. Application of an exogenous global agonist impairs working memory function. (*A*) Network profile of persistent activity averaged over 150 trials, 6 s into the delay period. A global agonist broadens the mnemonic activity pattern (red) compared with control (black). (*B*) Endpoints of memory-guided saccades, at the end of a 12-s delay period (see Methods). Saccades that fall outside of the large circles surrounding the sensory cue locations are considered as erroneous responses. Saccade endpoints are color coded by the cue location. (*C*) Variance of the remembered location during delay period, calculated from 50 trials, with (red) and without (black) a global agonist. In the presence of an exogenous activity-independent agonist, there is no DSI effect to stabilize random drifts, so the accuracy of memory-guided saccades deteriorates.

examine how global application of exogenous cannabinoid might alter network performance. This was done by assuming that a drug-like marijuana saturates the DSI effect, so that D is clamped to D_{min} for all pyramidal cells. We found that if $D = D_{min}$ is below a critical value, the network became too excitable and spontaneously generates a bump state without an external input. To increase the stability of the baseline state, in this set of simulations, we slightly increased the strength of synaptic connections from the inhibitory population to the excitatory population (see Methods). With this parameter change and a modest DSI effect ($D_{min} = 0.985$), we simulated the application of a bulk agonist by globally setting $D = D_{min}$. Figure 6*A* shows a mnemonic persistent activity pattern at the end of a delay period, which is broader with agonist application (red), than in control (black). To assess the effect of a global agonist on behavioral performance, we calculated the endpoints of 50 memory-guided saccades for each of 8 cues (Fig. 6*B*). In the plot, correct responses are defined as those inside the large thin circles. It is clear that saccade endpoints are much more varied when DSI is saturated. This is because with a global agonist, activity pattern in the network no longer creates a privileged position, so the noise moves the bump around randomly as in the model without DSI. As a result, the variance of the memory-guided saccades is significantly larger (Fig. 6*C*), similar to the observation of Ploner et al. (2002) with exposure to THC by human subjects.

Discussion

In this work, we developed a phenomenological model of cannabinoid-mediated DSI and explored its consequences in a network model of spatial working memory. DSI resulted in an activity-dependent, localized, and slowly recovering well of disinhibition for those neurons actively engaged in maintaining working memory. This privileged locus in the network limits random drifts of a persistent activity pattern and enhances memory robustness in the face of deleterious effects of adaptation. It also yields a lingering trace of disinhibition even after a mnemonic spiking activity is terminated, leading to trial-to-trial correlations in the behavioral responses. Finally, we found that simulated application of an exogenous agonist resulted in an increased variation of the memory-guided saccades, consistent with the observations from a human study (Ploner et al. 2002). Although we explored the DSI effect using a network model of spatial working memory, insights thus gained are relevant generally to any strongly recurrent neural

circuits, for which the collective dynamics critically depends on the interplay between multiple activity–dependent positive and negative feedback processes (synaptic excitation and inhibition, spike-frequency adaptation, DSI, etc.) with time constants ranging from milliseconds to seconds.

Cannabinoid-Mediated DSI

We introduced in this paper, a phenomenological model of the cannabinoid-mediated DSI with parameters calibrated by physiological data (Wang and Zucker 2001). We found that the overall maximum DSI effect should be small, roughly below 5%, otherwise the network tends to be unstable. This conclusion seems plausible, given that endocannabinoid signaling is primarily mediated by CCK interneurons, which constitute only a small fraction of all interneurons projecting to pyramidal cells.

Currently, it is still a matter of debate as to the size of endocannabinoid-mediated disinhibition that can be produced under physiological conditions. Many studies were done with membrane potential depolarization as induction protocol, rather than spike trains. However, Pitler and Alger (1992) showed, in hippocampal CA1, that disinhibition effect could be triggered using a spike train at 20 Hz for 2 s, which is quite comparable to the kind of sustained neural activity relevant to working memory function. A related question concerns the intracellular calcium concentration that is required for DSI induction (Brenowitz et al. 2006). Wang and Zucker (2001) reported a calcium concentration of 4 μM for half-maximum synaptic suppression (see Fig. 1*B*). Assuming a linear relationship between the firing rate and the resulting calcium accumulation, with a slope of 16 nM/Hz (Helmchen et al. 1996) and a persistent activity at 40 Hz, the expected calcium level is 0.64 μM, implying only a small disinhibition effect. This estimate does not consider other factors such as calcium release from internal stores (Isokawa and Alger 2006) or cholinergic modulation (Pitler and Alger 1992; Trettel and Levine 2003; Fortin et al. 2004) that could enhance the DSI effect. Regardless, our work suggests that even a few percent suppression of synaptic inhibition, provided it is spatially local and long lasting, could have a significant functional impact in a highly recurrent neural circuit of working memory.

Random Drifts in Continuous Attractor Networks

In our model, the main driving force that sustains a persistent activity pattern is the recurrent synaptic excitation. The elevated and long-lasting spike discharges in pyramidal neurons are the prerequisite for the induction of disinhibition. Moreover, activity dependence of this effect is crucial for dynamically creating, on the fly, a privileged locus in an a priori perfectly homogeneous network. This well of disinhibition "traps" and stabilizes a mnemonic activity pattern. This effect is especially interesting for continuous attractor networks, which typically exhibit random drifts of a persistent activity pattern. One possible solution is to increase the number of synaptic connections per neuron in the network: when there are more converging inputs onto a neuron, synaptic noise is averaged out, so that random drifts are reduced (Compte et al. 2000; Renart et al. 2003). However, this scenario does not seem to be compatible with the observation that mnemonic persistent activity of PFC neurons is indeed highly irregular (Compte et al. 2003). Therefore, other mechanisms for limiting random drifts seem required.

We showed that the inclusion of DSI prevents such drifts from growing after the initial 2 s during a mnemonic delay period. Interestingly, one study with behaving monkeys found that the variance of memory-guided saccades indeed plateaus for delays longer than 2–3 s (White et al. 1994), as predicted by our model. On the other hand, the original study of Funahashi (1989) appears to show a larger variability of saccade endpoints after a delay of 6 s than after 3 s. Also, Ploner et al. (1998) indicate that variability of memory-guided saccades in human subjects stops increasing only for delays longer than 20 s. The neuronal origin of the observed decrease of memory accuracy over time is unknown. We suggest that this gradual forgetting of working memory at the behavioral level is caused by random drifts of persistent activity, a model prediction that remains to be tested experimentally.

Random drifts are expected to be a characteristic of other types of continuous attractors, including memory circuits in which neural tuning curves are monotonic rather than Gaussian with respect to the encoded stimulus feature (Seung 1996; Romo et al. 1999; Koulakov et al. 2002; Miller et al. 2003; Machens et al. 2005; Miller and Wang 2006a). We have shown previously that neural activity in such a model network exhibits random walk and power-law fluctuations (Miller and Wang 2006b). It will be interesting to see, in future work, whether DSI reduces random-walk-type variability and improves memory-guided behavior in such circuits as well.

Slow DSI Dynamics

Another desirable feature of DSI effect is its slow time course. In a highly recurrent neural network, the relative speeds of positive and negative feedbacks are of the ultimate importance to functional stability. An example to the point is SRA with a time constant of ~100 ms. As a negative feedback mechanism SRA could, in principle, help control the firing rate of persistent activity in spite of exuberant recurrent excitation in a working memory network. However, modeling studies showed that SRA in interaction with fast (tens of milliseconds) recurrent excitation readily leads to oscillatory instability, as is intuitively expected for a highly nonlinear dynamical system with a fast-positive feedback followed by a slower negative feedback (Wang 1999, 2001). Better suited for counterbalancing SRA is a slower positive feedback process, such as DSI or short-term facilitation of excitatory synapses which has a time constant up to seconds and appears to be prominent in the PFC (Hempel et al. 2000; Wang et al. 2006).

The slow onset of DSI also provides a cellular mechanism for a ramping neural activity that builds up for seconds during a delay period (data not shown). Such ramping activity is commonly observed in prefrontal neurons in ODR experiments (Funahashi et al. 1989; Chafee and Goldman-Rakic 1998; Constantinidis et al. 2001; Takeda and Funahashi 2002), constituting ~38% of recorded neurons in one study (Chafee and Goldman-Rakic 1998). Ramping activity is also common in neurons with monotonic tuning of a remembered stimulus cue (Romo et al. 1999; Brody et al. 2003; Miller et al. 2003; Singh and Eliasmith 2006). Such ramping activity may be useful for specific computations like anticipation of the direction of an impending saccade, rather than retrospective memory of a previously presented cue (Takeda and Funahashi 2002) or timing of an anticipated behavioral response (Brody et al. 2003).

Furthermore, we showed that DSI in the network leaves a subthreshold memory trace across trials. This is interesting

because in laboratory experiments, neural activity recorded from behaving monkeys typically decays away at the end of each behavioral trial, yet behavioral responses often exhibit trial-to-trial correlations (Fecteau and Munoz 2003). It has not yet been examined whether such cross-trial–correlated behavior also holds true for the ODR task. In a study using a decision-making paradigm, both activity of prefrontal neurons and behavioral response in a given trial often exhibits a dependence on what happened in a previous trial (Barraclough et al. 2004). Two scenarios are conceivable: either neurons in certain brain regions exhibit persistent activity across intertrial intervals or the memory trace is not observable at the level of spiking discharges. We suggest that a subthreshold mechanism of the latter type may be instantiated by endocannabinoid signaling. If so, the size of cross-trial correlation should depend on the intertrial interval length relative to the time constant of DSI, a prediction that can be evaluated in monkey experiments. Our model can also be directly tested by pharmacological manipulation of CB1 receptors or CCK neurons in a spatial working memory circuit.

Exogenous Global Agonist

When we simulated application of an exogenous CB1 agonist, we found that the network lost resistance to random drift, and the variance of remembered location grows linearly during the entire delay period. Therefore, our model sheds insight into the observed THC effects on delayed oculomotor behavior (Ploner et al. 2002). A model prediction at the physiological level is an increase in the width of the network activity profile during the delay period, with global agonist application. Because both an antagonist and agonist would eliminate the primary DSI effect (localized disinhibition), we need to identify ways to tell them apart. When an agonist is administered, the tuning curves of the cells broaden and the variance in the memory-guided saccades is expected to increase. However, the saccade endpoints would still be scattered around the cue location. On the other hand, in the case of a systemically administered antagonist, our model predicts that spike-frequency adaptation, if significantly present in memory neurons, would render persistent activity unstable and would cause more failures in the delay period. Consequently, the saccade endpoints would be random and essentially uncorrelated with the cue location. These specific predictions are experimentally testable.

Concluding Remarks

In summary, because endocannabinoid-mediated DSI has a slow onset and requires long-lasting neural activity, it is ideally suited for influencing working memory, and perhaps decision-making, processes subserved by persistent neural activity. This is in contrast to rapid and brief neural activity in early sensory areas, which is likely not sufficient to induce DSI. This may, at least in part, explain why CB1 receptors are densely expressed in association cortices like the PFC, but not in early sensory areas. Furthermore, we showed that persistent neural activity in a model of spatial working memory is prone to random drifts, which can be dynamically contained by DSI. This is true not just for working memory of analog quantities but for continuous attractor networks in general. In particular, spatial navigation is believed to be subserved by continuous attractor dynamics in the entorhinal cortex and hippocampus (see McNaughton et al. [2006] and references therein), but the issue of random drifts remains a serious challenge to this theoretical framework (Song and Wang 2005; Burak and Fiete 2006). Because hippocampus is another brain region with a high expression of CB1 receptors, endocannabinoid may contribute to hippocampal functions by limiting random drifts of neural activity in the hippocampus system. This, however, may be only one of multiple CB1 actions. It is known that CCK neurons and CB1 receptors, play an important role in sculpturing rhythmic neural activity in the hippocampus (Klausberger et al. 2005; Robbe et al. 2006). The modulatory effects of endocannabinoid signaling on temporal aspects of neural firing patterns remains to be explored in computational models.

Funding

National Institute of Health (MH62349, DA016455).

Notes

We thank Paul Miller and Christos Constantinidis for helpful comments on the manuscript. *Conflict of Interest*: None declared.

Address correspondence to email: xjwang@yale.edu.

References

Alger BE, Pitler TA. 1995. Retrograde signaling at GABAA-receptor synapses in the mammalian CNS. Trends Neurosci. 18:333–340.

Amari S. 1977. Dynamics of pattern formation in lateral-inhibition type neural fields. Biol Cybern. 27:77–87.

Ameri A. 1999. The effects of cannabinoids on the brain. Prog Neurobiol. 58:315–348.

Barraclough DJ, Conroy ML, Lee D. 2004. Prefrontal cortex and decision making in a mixed-strategy game. Nat Neurosci. 7:404–410.

Ben-Yishai R, Bar-Or RL, Sompolinsky H. 1995. Theory of orientation tuning in visual cortex. Proc Natl Acad Sci USA. 92:3844–3848.

Bodor AL, Katona I, Nyíri G, Mackie K, Ledent C, Hájos N, Freund TF. 2005. Endo-cannabinoid signaling in rat somatosensory cortex: laminar differences and involvement of specific interneuron types. J Neurosci. 25:6845–6856.

Brenowitz SD, Best AR, Regehr WG. 2006. Sustained elevation of dendritic calcium evokes widespread endocannabinoid release and suppression of synapses onto cerebellar Purkinje cells. J Neurosci. 26:6841–6850.

Brenowitz SD, Regehr WG. 2003. Calcium dependence of retrograde inhibition by endocannabinoids at synapses onto Purkinje cells. J Neurosci. 23:6373–6384.

Brody CD, Hernandez A, Zainos A, Romo R. 2003. Timing and neural encoding of somatosensory parametric working memory in macaque prefrontal cortex. Cereb Cortex. 13:1196–1207.

Burak Y, Fiete I. 2006. Do we understand the emergent dynamics of grid cell activity? J Neurosci. 26:9352–9354.

Camperi M, Wang X-J. 1998. A model of visuospatial working memory in prefrontal cortex: recurrent network and cellular bistability. J Comput Neurosci. 5:383–405.

Chafee MV, Goldman-Rakic PS. 1998. Matching patterns of activity in primate prefrontal area 8a and parietal area 7ip neurons during a spatial working memory task. J Neurophysiol. 79:2919–2940.

Compte A, Brunel N, Goldman-Rakic PS, Wang X-J. 2000. Synaptic mechanisms and network dynamics underlying spatial working memory in a cortical network model. Cereb Cortex. 10:910–923.

Compte A, Constantinidis C, Tegner J, Raghavachari S, Chafee M, Goldman-Rakic PS, Wang X-J. 2003. Temporally irregular mnemonic persistent activity in prefrontal neurons of monkeys during a delayed response task. J Neurophysiol. 90:3441–3454.

Connors BW, Gutnick MJ, Prince DA. 1982. Electrophysiological properties of neocortical neurons *in vitro*. J Neurophysiol. 48:1302–1320.

Constantinidis C, Franowicz MN, Goldman-Rakic PS. 2001. Coding specificity in cortical microcircuits: a multiple-electrode analysis of primate prefrontal cortex. J Neurosci. 21:3646–3655.

Constantinidis C, Wang X-J. 2004. A neural circuit basis for spatial working memory. Neuroscientist. 10:553–565.
Courtney SM, Petit L, Maisog JM, Ungerleider LG, Haxby JV. 1998. An area specialized for spatial working memory in human frontal cortex. Science. 279:1347–1351.
Dean B, Sundram S, Bradbury R, Scarr E, Copolov D. 2001. Studies on [3h]cp-55940 binding in the human central nervous system: regional specific changes in density of cannabinoid-1 receptors associated with schizophrenia and cannabis use. Neuroscience. 103:9–15.
Di Marzo V, Fontana A, Cadas H, Schinelli S, Cimino G, Schwartz JC, Piomelli D. 1994. Formation and inactivation of endogenous cannabinoid anandamide in central neurons. Nature. 372:686–691.
Eggan SM, Lewis DA. 2007. Immunocytochemical distribution of the cannabinoid cb1 receptor in the primate neocortex: a regional and laminar analysis. Cereb Cortex. 17:175–191.
Fecteau JH, Munoz DP. 2003. Exploring the consequences of the previous trial. Nat Rev Neurosci. 4:435–443.
Foehring RC, Lorenzon NM, Herron P, Wilson CJ. 1991. Correlation of physiologically and morphologically identified neuronal types in human association cortex *in vitro*. J Neurophysiol. 66:1825–1837.
Fortin DA, Trettel J, Levine ES. 2004. Brief trains of action potentials enhance pyramidal neuron excitability via endocannabinoid-mediated suppression of inhibition. J Neurophysiol. 92:2105–2112.
Freund TF, Katona I, Piomelli D. 2003. Role of endogenous cannabinoids in synaptic signaling. Physiol Rev. 83:1017–1066.
Funahashi S, Bruce CJ, Goldman-Rakic PS. 1989. Mnemonic coding of visual space in the monkey's dorsolateral prefrontal cortex. J Neurophysiol. 61:331–349.
Fuster JM. 1973. Unit activity in prefrontal cortex during delayed-response performance: neuronal correlates of transient memory. J Neurophysiol. 36:61–78.
Georgopoulos AP, Kalaska JF, Caminiti R, Massey JT. 1982. On the relations between the direction of two-dimensional arm movements and cell discharge in primate motor cortex. J Neurosci. 2:1527–1537.
Glass M, Dragunow M, Faull RL. 1997. Cannabinoid receptors in the human brain: a detailed anatomical and quantitative autoradiographic study in the fetal, neonatal and adult human brain. Neuroscience. 77:299–318.
Gnadt JW, Andersen RA. 1988. Memory related motor planning activity in posterior parietal cortex of macaque. Exp Brain Res. 70:216–220.
Goldman-Rakic PS. 1995. Cellular basis of working memory. Neuron. 14:477–485.
Hajos N, Katona I, Naiem SS, MacKie K, Ledent C, Mody I, Freund TF. 2000. Cannabinoids inhibit hippocampal GABAergic transmission and network oscillations. Eur J Neurosci. 12:3239–3249.
Hampson RE, Deadwyler SA. 2000. Cannabinoids reveal the necessity of hippocampal neural encoding for short-term memory in rats. J Neurosci. 20:8932–8942.
Hansel D, Mato G, Meunier C, Neltner L. 1998. On numerical simulations of integrate-and-fire neural networks. Neural Comput. 10:467–483.
Hansel D, Sompolinsky H. 1998. Modeling feature selectivity in local cortical circuits, chapter 13. 2nd ed. Cambridge: MIT Press.
Heinbockel T, Brager DH, Reich CG, Zhao J, Muralidharan S, Alger BE, Kao JP. 2005. Endocannabinoid signaling dynamics probed with optical tools. J Neurosci. 25:9449–9459.
Helmchen F, Imoto K, Sakmann B. 1996. Ca2+ buffering and action potential-evoked Ca2+ signaling in dendrites of pyramidal neurons. Biophys J. 70:1069–1081.
Hempel CM, Hartman KH, Wang X-J, Turrigiano GG, Nelson SB. 2000. Multiple forms of short-term plasticity at excitatory synapses in rat medial prefrontal cortex. J Neurophysiol. 83:3031–3041.
Hoffman AF, Lupica CR. 2000. Mechanisms of cannabinoid inhibition of GABA(A) synaptic transmission in the hippocampus. J Neurosci. 20:2470–2479.
Ilan AB, Smith ME, Gevins A. 2004. Effects of marijuana on neurophysiological signals of working and episodic memory. Psychopharmacology (Berl). 176:214–222.
Isokawa M, Alger BE. 2006. Ryanodine receptor regulates endogenous cannabinoid mobilization in the hippocampus. J Neurophysiol. 95:3001–3011.
Katona I, Sperlagh B, Sik A, Kafalvi A, Vizi ES, Mackie K, Freund TF. 1999. Presynaptically located CB1 cannabinoid receptors regulate GABA release from axon terminals of specific hippocampal interneurons. J Neurosci. 19:4544–4558.
Kikuchi-Yorioka Y, Sawaguchi T. 2000. Parallel visuospatial and audiospatial working memory processes in the monkey dorsolateral prefrontal cortex. Nat Neurosci. 3:1075–1076.
Klausberger T, Marton LF, O'Neill J, Huck JH, Dalezios Y, Fuentealba P, Suen WY, Papp E, Kaneko T, Watanabe M, et al. 2005. Complementary roles of cholecystokinin- and parvalbumin-expressing gabaergic neurons in hippocampal network oscillations. J Neurosci. 25:9782–9793.
Koch G, Oliveri M, Torriero S, Carlesimo GA, Turriziani P, Caltagirone C. 2005. rTMS evidence of different delay and decision processes in a fronto-parietal neuronal network activated during spatial working memory. Neuroimage. 24:34–39.
Koulakov AA, Raghavachari S, Kepecs A, Lisman JE. 2002. Model for a robust neural integrator. Nat Neurosci. 5:775–782.
Kreitzer AC, Carter AG, Regehr WG. 2002. Inhibition of interneuron firing extends the spread of endocannabinoid signaling in the cerebellum. Neuron. 34:787–796.
Kreitzer AC, Regehr WG. 2001. Retrograde inhibition of presynaptic calcium influx by endogenous cannabinoids at excitatory synapses onto Purkinje cells. Neuron. 29:717–727.
Laing CR, Longtin A. 2001. Noise-induced stabilization of bumps in systems with long-range spatial coupling. Physica D. 160:149–172.
Lenz RA, Alger BE. 1999. Calcium dependence of depolarization-induced suppression of inhibition in rat hippocampal CA1 pyramidal neurons. J Physiol. 521(Pt 1):147–157.
Liu YH, Wang X-J. 2001. Spike-frequency adaptation of a generalized leaky integrate-and-fire model neuron. J Comput Neurosci. 10:25–45.
Llano I, Leresche N, Marty A. 1991. Calcium entry increases the sensitivity of cerebellar Purkinje cells to applied GABA and decreases inhibitory synaptic currents. Neuron. 6:565–574.
Lorenzon NM, Foehring RC. 1992. Relationship between repetitive firing and afterhyperpolarizations in human neocortical neurons. J Neurophysiol. 67:350–363.
Machens CK, Romo R, Brody CD. 2005. Flexible control of mutual inhibition: a neural model of two-interval discrimination. Science. 307:1121–1124.
Marsicano G, Lutz B. 1999. Expression of the cannabinoid receptor cb1 in distinct neuronal subpopulations in the adult mouse forebrain. Eur J Neurosci. 11:4213–4225.
Mason A, Larkman A. 1990. Correlations between morphology and electrophysiology of pyramidal neurons in slices of rat visual cortex. II. Electrophysiology. J Neurosci. 10:1415–1428.
McCarthy G, Blamire AM, Puce A, Nobre AC, Bloch G, Hyder F, Goldman-Rakic PS, Shulman RG. 1994. Functional magnetic resonance imaging of human prefrontal cortex activation during a spatial working memory task. Proc Natl Acad Sci USA. 91:8690–8694.
McCormick DA, Connors BW, Lighthall JW, Prince DA. 1985. Comparative electrophysiology of pyramidal and sparsely spiny stellate neurons of the neocortex. J Neurophysiol. 54:782–806.
McNaughton BL, Battaglia FP, Jensen O, Moser EI, Moser MB. 2006. Path integration and the neural basis of the 'cognitive map'. Nat Rev Neurosci. 7:663–678.
Miller P, Brody CD, Romo R, Wang XJ. 2003. A recurrent network model of somatosensory parametric working memory in the prefrontal cortex. Cereb Cortex. 13:1208–1218.
Miller P, Wang X-J. 2006a. Inhibitory control by an integral feedback signal in prefrontal cortex: a model of discrimination between sequential stimuli. Proc Natl Acad Sci USA. 103:201–206.
Miller P, Wang X-J. 2006b. Power-law neuronal fluctuations in a recurrent network model of parametric working memory. J Neurophysiol. 95:1099–1114.
Müri RM, Vermersch AI, Rivaud S, Gaymard B, Pierrot-Deseilligny C. 1996. Effects of single-pulse transcranial magnetic stimulation over the prefrontal and posterior parietal cortices during memory-guided saccades in humans. J Neurophysiol. 76:2102–2106.
Niki H, Watanabe M. 1976. Prefrontal unit activity and delayed response: relation to cue location versus direction of response. Brain Res. 105:79–88.

Ohno-Shosaku T, Maejima T, Kano M. 2001. Endogenous cannabinoids mediate ret rograde signals from depolarized postsynaptic neurons to presynaptic terminals. Neuron. 29:729–738.
Oliveri M, Turriziani P, Carlesimo GA, Koch G, Tomaiuolo F, Panella M, Caltagirone C. 2001. Parieto-frontal interactions in visual-object and visual-spatial working memory: evidence from transcranial magnetic stimulation. Cereb Cortex. 11:606–618.
Ong WY, Mackie K. 1999. A light and electron microscopic study of the cb1 cannabinoid receptor in primate brain. Neuroscience. 92:1177–1191.
Pinto DJ, Ermentrout GB. 2001a. Spatially structured activity in synaptically coupled neuronal networks: I. Traveling fronts and pulses. SIAM J Appl Math. 62:206–225.
Pinto DJ, Ermentrout GB. 2001b. Spatially structured activity in synaptically coupled neuronal networks: II. Lateral inhibition and standing pulses. SIAM J Appl Math. 62:226–243.
Piomelli D. 2003. The molecular logic of endocannabinoid signalling. Nat Rev Neurosci. 4:873–884.
Pitler TA, Alger BE. 1992. Postsynaptic spike firing reduces synaptic GABAA responses in hippocampal pyramidal cells. J Neurosci. 12:4122–4132.
Ploner CJ, Gaymard B, Rivaud S, Agid Y, Pierrot-Deseilligny C. 1998. Temporal limits of spatial working memory in humans. Eur J Neurosci. 10:794–797.
Ploner CJ, Tschirch A, Ostendorf F, Dick S, Gaymard BM, Rivaud-Pechoux S, Sporkert F, Pragst F, Stadelmann AM. 2002. Oculomotor effects of delta-9-tetrahydrocannabinol in humans: implications for the functional neuroanatomy of the brain cannabinoid system. Cereb Cortex. 12:1016–1023.
Rainer G, Asaad WF, Miller EK. 1998. Memory fields of neurons in the primate prefrontal cortex. Proc Natl Acad Sci USA. 95: 15008–15013.
Renart A, Song P, Wang XJ. 2003. Robust spatial working memory through homeostatic synaptic scaling in heterogeneous cortical networks. Neuron. 38:473–485.
Robbe D, Montgomery SM, Thome A, Rueda-Orozco PE, McNaughton BL, Buzsaki G. 2006. Cannabinoids reveal importance of spike timing coordination in hippocampal function. Nat Neurosci. 9:1526–1533.
Romo R, Brody CD, Hernandez A, Lemus L. 1999. Neuronal correlates of parametric working memory in the prefrontal cortex. Nature. 399:470–473.
Sawaguchi T, Iba M. 2001. Prefrontal cortical representation of visuo-spatial working memory in monkeys examined by local inactivation with muscimol. J Neurophysiol. 86:2041–2053.
Sawaguchi T, Yamane I. 1999. Properties of delay-period neuronal activity in the monkey dorsolateral prefrontal cortex during a spatial delayed matching-to-sample task. J Neurophysiol. 82:2070–2080.
Schiller J, Helmchen F, Sakmann B. 1995. Spatial profile of dendritic calcium transients evoked by action potentials in rat neocortical pyramidal neurones. J Physiol. 487(Pt 3):583–600.
Seung HS. 1996. How the brain keeps the eyes still. Proc Natl Acad Sci USA. 93:13339–13344.
Singh R, Eliasmith C. 2006. Higher-dimensional neurons explain the tuning and dynamics of working memory cells. J Neurosci. 26:3667–3678.
Song P, Wang XJ. 2005. Angular path integration by moving "hill of activity": a spiking neuron model without recurrent excitation of the head-direction system. J Neurosci. 25:1002–1014.
Stella N, Schweitzer P, Piomelli D. 1997. A second endogenous cannabinoid that modulates long-term potentiation. Nature. 388:773–778.
Takeda K, Funahashi S. 2002. Prefrontal task-related activity representing visual cue location or saccade direction in spatial working memory tasks. J Neurophysiol. 87:567–588.
Thayer SA, Miller RJ. 1990. Regulation of the intracellular free calcium concentration in single rat dorsal root ganglion neurones *in vitro*. J Physiol. 425:85–115.
Trettel J, Levine ES. 2003. Endocannabinoids mediate rapid retrograde signaling at interneuron → pyramidal neuron synapses of the neocortex. J Neurophysiol. 89:2334–2338.
Tuckwell HC. 1988. Introduction to theoretical neurobiology. Cambridge: Cambridge University Press.
van Vreeswijk C, Hansel D. 2001. Patterns of synchrony in neural networks with spike adaptation. Neural Comput. 13:959–992.
Wang J, Zucker RS. 2001. Photolysis-induced suppression of inhibition in rat hippocampal CA1 pyramidal neurons. J Physiol. 533:757–763.
Wang X-J. 1999. Synaptic basis of cortical persistent activity: the importance of NMDA receptors to working memory. J Neurosci. 19:9587–9603.
Wang X-J. 2001. Synaptic reverberation underlying mnemonic persistent activity. Trends Neurosci. 24:455–463.
Wang X-J. 2006. A microcircuit model of prefrontal functions: ying and yang of reverberatory neurodynamics in cognition. In: Risberg J, Grafman J, editors. The prefrontal lobes: development, function and pathology. New York: Cambridge University Press. p. 92–127.
Wang X-J, Liu Y, Sanchez-Vives MV, McCormick DA. 2003. Adaptation and temporal decorrelation by single neurons in the primary visual cortex. J Neurophysiol. 89:3279–3293.
Wang Y, Markram H, Goodman PH, Berger TK, Ma J, Goldman-Rakic PS. 2006. Heterogeneity in the pyramidal network of the medial prefrontal cortex. Nat Neurosci. 9:534–542.
White JM, Sparks DL, Stanford TR. 1994. Saccades to remembered target locations: an analysis of systematic and variable errors. Vision Res. 34:79–92.
Wilson RI, Kunos G, Nicoll RA. 2001. Presynaptic specificity of endocannabinoid signaling in the hippocampus. Neuron. 31:453–462.
Wilson RI, Nicoll RA. 2001. Endogenous cannabinoids mediate retrograde signalling at hippocampal synapses. Nature. 410:588–592.
Wilson RI, Nicoll RA. 2002. Endocannabinoid signaling in the brain. Science. 296:678–682.
Zarahn E, Aguirre GK, D'Esposito M. 1999. Temporal isolation of the neural correlates of spatial mnemonic processing with fMRI. Brain Res Cogn Brain Res. 7:255–268.